Revision 1

Word count: 7072

Interplay between fluid circulation and Alpine metamorphism in the Monte Rosa whiteschist from white mica and quartz in situ oxygen isotope analysis by SIMS.

Luisier Cindy (1,2)*, Lukas P. Baumgartner (1), Anne-Sophie Bouvier (1) and Benita Putlitz (1)

(1) Institute of Earth Sciences, University of Lausanne, 1015 Lausanne, Switzerland +41216924446

(2) Univ Rennes, CNRS, Géosciences Rennes UMR 6118, Rennes, France +33223236783

* Corresponding author e-mail: cindy.luisier@unil.ch

Abstract

In-situ oxygen isotope compositions of white mica and quartz have been used to characterize the interplay of metamorphism and fluid events between a metasomatic whiteschist and its granite protolith in the Monte Rosa nappe, Western Alps. New natural muscovite and phengites reference materials were calibrated for in-situ Secondary Ion Mass Spectrometry (SIMS) oxygen isotope measurement. White mica and quartz oxygen isotope compositions were measured in situ in one whiteschist and two metagranite. Based on microtextural observation, phengite composition of white mica and phase petrology modelling, it is possible to identify two events of fluid infiltration, and one event of fluid expulsion, which were responsible to

form this unique whiteschist occurrence and to trace its metamorphic evolution from late Permian intrusion to Alpine subduction and finally to the present day, exhumed whiteschist.

Metagranite samples contain three generations of white mica: igneous, high-P metamorphic, and late Alpine, retrograde compositions. In the whiteschist samples, we distinguish two distinct Alpine white mica generations, a first, prograde to peak generation and a second, retrograde generation.

The $\delta^{18}O_{VSMOW}$ values of white mica and quartz from a whiteschist of 5.3 to 7.3‰ and 9.1 to 10.6‰ are significantly lower than in the metagranites, with 9.1 to 10.8‰ and 13.2 to 14.6‰ respectively. This indicates a complete recrystallization of the whiteschist protolith during intense fluid-rock interaction. Subsequent Alpine metamorphism transformed the protolith into the whiteschist. The isotopic composition of the whiteschist fine-grained retrograde white mica (5.3 to 6‰) is lower than that of the high-pressure phengite (6.2 and 7.5‰). The low $\delta^{18}O$ values could be explained by infiltration of external fluids with $\delta^{18}O$ values of 2 to 6‰. Such fluids would carry the isotopic signature of the serpentinites of the Piedmont ocean by either equilibration of fluids with or dehydration of serpentinites. Another, more simple explanation would be infiltration of very small quantity of fluids leading to the breakdown of the chloritoid. Local inheritance of the oxygen composition would then hide the origin of the fluids.

Isotope exchange temperatures calculated from high-P phengite-quartz pairs in whiteschist give an average temperature of 440 ± 50 °C. These are lower than the best T-estimates from phase petrology of 570 °C, at 2.2 GPa. Igneous muscovite-quartz pairs in the metagranite yield 400 ± 40 °C. Only one high-P phengite/quartz pair was analyzed, resulting in 350 ± 40 °C. Greenschist facies low-silica phengites give an average temperature of 310 ± 10 °C. Propagation of analytical uncertainty suggests large errors of 60 °C to 120 °C, due to the relatively small T-dependence of the quartz-white mica fractionation factor for oxygen isotopes.

Introduction

White mica is stable under a wide range of pressure (P) and temperature (T) conditions (Bailey, 1984). It participates in many important dehydration and melting reactions in regional and contact metamorphic environments (e.g., Gardien et al., 2000; Pattison and Harte, 1991; Skora and Blundy, 2010; Spear, 1995), and is a tracer of fluid flow in hydrothermal systems (e.g., Bulle et al., 2020). The growing understanding of their chemico-mechanical behavior during orogenic processes allow a characterization of the conditions under which they crystallize and deform. Notably, the phengite solid solution series has attracted much interest in the field of geothermobarometry, since individual substitutions are controlled by pressure and temperature conditions in buffered systems (Spear, 1995). As an example, the Tschermak substitution of (Mg, Fe) + Si against 2Al is known to be promoted by an increase in pressure, which led to the initial experimental determination of the silica in phengite barometer by Massonne and Schreyer (1987). Oxygen isotopes thermometry using quartz-muscovite or quartz-phengite (e.g., Eslinger et al., 1979; Zheng, 1993) has also facilitated the temperature estimation, as they are present in association in most rock types. Other applications of oxygen isotopes in white mica in the domain of fluid-rock interactions include hydrothermal fluid characterization (Bulle et al., 2020).

Oxygen isotope analyses by laser fluorination techniques are precise (± 0.1‰ 1 sigma), but requires time intensive, careful mineral separation; a task made difficult especially in polymetamorphic rocks, where several generations of the same mineral can coexist. In addition, imperfect mineral species separations, by for example the presence of various inclusions, can introduce a bias in the isotopic signal of any given mineral, rendering thermometry and interpretation of oxygen isotope signal spurious. In-situ stable isotopes measurement by Secondary Ion Mass Spectrometry (SIMS) has improved our capability of observing the spatial

relationship between the analyzed phases and promotes a better in depth understanding of the data obtained. To take advantage of this technique, it is paramount to have matrix matched reference materials (e.g., Marger et al., 2019; Siron et al., 2017; Valley and Kita, 2009). The minimization of surface topography during sample preparation as well as the use of isotopically homogeneous reference materials has increased the analytical precision over the years, allowing a wide range of geological materials to be studied (e.g., Kita et al., 2011; Valley and Kita, 2009). To our knowledge, white mica reference materials have been missing in the petrology toolbox so far. Therefore, we describe and characterize 4 white mica standards, which cover a wide range of celadonite content, designed to analyze phengitic muscovites.

The white mica standards are applied to the study of whiteschists from the Monte Rosa nappe (Western European Alps), which have been the focus of numerous studies (Chopin and Monié, 1984; Le Bayon et al., 2006; Luisier et al., 2021, 2019; Marger et al., 2019). Whiteschists have been defined by Schreyer (1973) as high-pressure, Mg and Al-rich rocks, in which the mineral association talc - kyanite or talc - chloritoid is commonly found (Chopin, 1985; Schreyer, 1974). The Monte Rosa whiteschist show the high pressure paragenesis of chloritoid, talc, phengite and quartz, with locally rare kyanite, garnet and carbonate. The origin of whiteschists in the Alps is still debated (Ferrando, 2012). While alteration by ultramafic derived fluids during prograde to peak Alpine conditions were proposed for the Dora-Maira whiteschist (see Ferrando, 2012 for a review), the genesis of the Monte Rosa whiteschists has been explained by metasomatic alteration of the granite by late magmatic hydrothermal fluids (Luisier et al., 2021; Pawlig and Baumgartner, 2001). Luisier et al. (2021) have demonstrated that the chemistry of the whiteschist was acquired before the onset of Alpine metamorphism. The mineral assemblages now observable in the whiteschist and metagranite result from a combination of Alpine metamorphism and the deformation relative to the nappe emplacement and exhumation.

In this study, we use white mica and quartz oxygen isotope compositions in metagranite and associated metasomatic whiteschist from the Monte Rosa nappe, in the Western Alps (Fig. 1A), to track the interplay between fluid fluxes and metamorphism. The aim is to combine white mica and quartz isotopic compositions with microstructural observations and major element compositions, in order to identify the potential extent and nature of fluid fluxes between a metasomatic whiteschist and its metagranite protolith during the Alpine history of the Monte Rosa nappe.

Geological setting

The Monte Rosa nappe is part of the Penninic domain of the Western Alps (Fig. 1A). It belongs to the Internal Crystalline Massifs, together with the Gran Paradiso and Dora Maira. From a paleogeographic point of view, it corresponds to the southernmost tip of the Briançonnais microcontinent and hence represents the deepest subducted part of the European continental crust involved in the Alpine orogeny (Steck et al., 2015). The nappe consists of a pre-Alpine polymetamorphic paragneiss unit, in which granodioritic to granitic bodies intruded during the Permian (Bearth, 1952; Dal Piaz, 2001), dated by SHRIMP U-Pb on zircon at 269 ± 4 Ma (Pawlig, 2001). The granite locally grades into 10 to 50 meters bodies of whiteschist (Fig. 1B). The whiteschists are metasomatic alteration products of the Monte Rosa granite. The metasomatism occurred pre-Alpine, likely during late hydrothermal alteration of the cooling granite intrusion (Luisier et al., 2021; Pawlig and Baumgartner, 2001). Subsequently, the mineralogy was produced during Alpine high-pressure metamorphism (Luisier et al., 2019; Marger et al., 2019). The peak high-pressure Alpine metamorphism has been dated at 42.6 ± 0.6 Ma (Lapen et al., 2007), by U/Pb geochronology on rutile in an eclogite of the Monte Rosa nappe. The P-T conditions for the peak metamorphism are estimated based on whiteschist phase

126 petrology between 1.6 to 2.7 GPa for a temperature range of 490 to 575 °C (Chopin and Monié,
127 1984; Le Bayon et al., 2006; Luisier et al., 2019). An age range between 42 to 39 Ma has been
128 found for the post-peak retrogression to upper greenschist facies (Skora et al., 2015), based on
129 Rb/Sr dating on phengite.
130 The study area is located to the North of the Mezzalama refuge, in the upper Ayas Valley, in
131 Italy. Here, the Alpine metamorphism is heterogeneously recorded through the nappe and
132 tightly related to the deformation intensity. Large volumes of rocks were very little deformed
133 during the nappe formation and exhumation. Deformation is concentrated in high strain areas,
134 such as thin shear zones as observed for example in the metagranite around the studied
135 whiteschist body (Vaughan-Hammon et al., 2021). Here, we focus on the whiteschist body
136 described in detail by Luisier et al. (2021), which is ellipsoidal. It is a cross-section through a
137 whiteschist pipe (Luisier et al., 2021, 2019). The central part of the whiteschist body consists
138 of an Alpine peak pressure mineral assemblage chloritoid, talc, phengite and quartz. Tiny
139 sericitic phengite and chlorite crystals are locally found as retrograde products after chloritoid
140 destabilization, attributed to the greenschist facies overprint. The transition between the
141 whiteschist body towards the metagranite occurs on a small distance, over a few tens of
142 centimeters to one meter, and is characterized by a completely retrogressed paragenesis, in
143 which the peak pressure whiteschist paragenesis is replaced by a greenschist facies mineral
144 assemblage consisting of chlorite, white mica and quartz.
145

146 # Analytical methods

147 **X-Ray Fluorescence (XRF)**

148 Fresh samples were selected and crushed with a hydraulic press. Rock fragments were
149 powdered in a tungsten carbide mill, dried in the oven at 110 °C and calcined at 1050 °C for
150 three hours. Loss on ignition (LOI) was calculated by weight difference after calcination.

Powders were mixed with lithium tetraborate ($Li_2B_4O_7$) and melted to produce glass pellets. The abundance of the major element oxides was determined by X-ray fluorescence using a PANalytical Axios-mAX spectrometer at Lausanne University, Switzerland. Ferrous iron was determined by colorimetric method in Lausanne University, Switzerland.

Electron Probe Microanalyzer (EPMA)

White micas covering part of the phengite compositional range were selected and tested for chemical homogeneity in major elements by EPMA (Table 1). Si, Ti, Al, Mg, Fe, K, Na, Ca, F and Cl content of white mica were measured using a JEOL JXA-8350F HyperProbe EPMA at Lausanne University, Switzerland. Operating conditions were 15 kV, 15 nA and a beam size of 5 µm. Natural minerals were used as standards. White mica structural formulae were obtained by normalization on a basis of 22 negative charges.

Laser fluorination (LF) for oxygen isotope analysis

The oxygen isotope composition of white mica reference materials was determined at the University of Lausanne (Switzerland) using the CO_2 laser fluorination technique (Lacroix and Vennemann, 2015) coupled with a Thermo Finnigan MAT 253 gas source mass spectrometer. White mica grain separates were loaded into Pt holders and dried in the oven at 110°C for ca. 12 hours before loading into the LF chamber. White mica SIMS reference materials were analyzed as replicates in several sessions. During each analytical session white mica aliquots were measured together with the NBS-28 qtz. White mica data are corrected to the session value of the NBS-28 quartz (accepted value of 9.64‰ as reported by Coplen et al. (1983). The repeatability of NBS-28 quartz determined as average of daily replicates is usually better than 0.1‰ (1SD). Data are given in conventional δ-notation, relative to Vienna Standard Mean Ocean Water (VSMOW).

This is the peer-reviewed, final accepted version for American Mineralogist, published by the Mineralogical Society of America.
The published version is subject to change. Cite as Authors (Year) Title. American Mineralogist, in press.
DOI: https://doi.org/10.2138/am-2020-7523. http://www.minsocam.org/

176

177 **Thermodynamic modelling**

178 The whiteschist 14MR67 whole rock composition with the following composition determined
179 by XRF is used for thermodynamic modelling: SiO_2: 66.13, TiO_2: 0.43, Al_2O_3: 15.85, Fe_2O_3:
180 1.75, FeO: 1.29, MnO: 0.02, MgO: 6.51, CaO: 0.17, Na_2O: 0.44, K_2O: 3.07, P_2O_5: 0.13, H_2O:
181 4.34. Since CaO, Na_2O, TiO_2, P_2O_5 and MnO are only present in minor amounts (< 0.5 wt%),
182 the simplified KFMASH system was used for thermodynamic modelling. All iron was assumed
183 to be ferrous. The composition used is (in moles): SiO_2(66.02), $AlO_{1.5}$(18.65), FeO(1.73),
184 MgO(9.69), $KO_{0.5}$(3.91). H_2O saturated conditions were assumed, since no carbonate phase
185 was observed in this whiteschist. Initial calculations revealed that carbonates become stable
186 with only minor amount of CO_2 (X_{CO2}<0.1), which do not significantly influence the P-T
187 conditions calculated by dehydration reactions (Bucher-Nurminen et al., 1983). Calculations
188 were performed using the internally consistent database of Berman (Berman, 1988, 92 update)
189 and Domino software (de Capitani and Brown, 1987). Solution models used are from Berman
190 (Berman, 1988), except for white mica (Massonne and Szpurka, 1997). To account for the small
191 amount of iron measured in talc (average X_{Mg} of 0.95), we adjusted the standard state
192 thermodynamic S^0 of Mg-talc in Berman's thermodynamic data as follow: $S^{T0,P0}_{Fe-MgTlc} =$
193 $S^{T0,P0}_{MgTlc} - R\ln(a)$, with $S^{T0,P0}_{Fe-MgTlc}$ being the standard state entropy of Fe-Mg-Talc at 25 °C
194 and 1 Bar, $S^{T0,P0}_{MgTlc}$ is the standard state entropy of pure Mg-Talc, R is the gas constant and a is
195 the activity of talc, calculated as: $a = (X_{Mg})^3$, with X_{Mg} = Mg/(Mg+Fe). The corrected standard
196 state S^0 is 262.5199 J/(K mol) for an average talc X_{Mg} of 0.95.

197

198 **Secondary Ion Mass Spectrometry (SIMS)**

199 White mica reference materials were mounted and polished in epoxy mounts together with the
200 biotite standard UNIL_B2 (Siron et al., 2017) for drift monitoring. The topography of the

mounts has been systematically checked using a white light interferometer and a maximum of 5 µm relief was accepted. Epoxy and indium mounts were cleaned using pure ethanol, dried in the oven at 60°C and stored in a vacuum desiccator. They were coated with 35 nm of gold.

In-situ oxygen isotopes measurements were conducted on a Cameca IMS 1280HR instrument in the SwissSIMS facility (University of Lausanne, Switzerland), using a focused high-density 1.5 nA Cs^+ primary beam at 10 kV in a Gaussian mode. A spot size of ~ 15 µm was achieved without rastering. An electron flood gun was used to compensate surface charge and was optimized before each session. An entrance slit of 122 µm and exit slit of 1346 µm allowed a mass resolution of ~ 2400. ^{16}O and ^{18}O were measured simultaneously in multi-collection mode on Faraday cups. Mass calibration, background correction and Faraday cups calibration were performed at the beginning of each session. The electron gun was tuned once a week. Counting statistics on 20 acquisition cycles for each analyzes gave an uncertainty precision in the order of 0.20‰ to 0.35‰ (2 standard errors, noted hereafter 2SE). A typical session was set with 4-6 UNIL_B2 standard analyses at the beginning, followed by one standard analysis each three unknown, in order to monitor drift. Drift was corrected if needed, by applying first or second order polynomial regressions based on the fit of reference material analyses. Intra-grain and inter-grain oxygen isotope variability of the reference materials was tested on a total of 5 to 10 grains from each species, randomly selected, by measuring 3 to 20 SIMS spot analyses on different regions within each grain (Supplementary material S1).

In order to determine any compositional related Instrumental Mass Fractionation (IMF), several grains of each species were mounted together in the same mount and measured in a calibration session with one of the reference materials as internal standard. Data were corrected for drift when needed. If the IMF is small (<20‰), it can be formulated following Equation 1 (Eiler et al., 1997; Siron et al., 2017):

$$\text{IMF (‰)} = \delta^{18}O_{\text{SIMS}} - \delta^{18}O_{\text{LF}} \quad (1)$$

Here, $\delta^{18}O_{SIMS}$ is the mean of measurements in a session of a reference material SIMS measurements, corrected for drift if necessary, and $\delta^{18}O_{LF}$ is the mean of all laser fluorination (LF) measurements for a given sample. IMF is calculated for each reference material and the ΔIMF is then calculated as the difference between the maximal and minimal IMF value among the four reference materials. The details of the development of the RM materials are discussed below.

The Monte Rosa thin sections were analyzed together with the new established white mica RM UNIL_WM3 (7.9 ± 0.09‰) and quartz RM UNIL-Q1 (9.8 ± 0.06‰; Seitz et al., 2017). Thin sections chips were pressed in indium together with cut epoxy pieces containing a polished white mica RM and a polished quartz RM. White mica and quartz $\delta^{18}O$ were measured in two different sessions, both using a primary beam of 1.5 nA, without raster.

Final uncertainty on each unknown SIMS measurement is calculated following Equation 2:

$$2\text{SE} = \sqrt{(2SE_{SIMS}^{unk})^2 + (2SD_{SIMS}^{RM})^2 + (2SD_{LF}^{RM})^2} \quad (2)$$

Where $2SE_{SIMS}^{unk}$ represents 2 times the standard error on the mean of the 20 cycles measured for each SIMS analyses, $2SD_{SIMS}^{RM}$ is 2 times the standard deviation on the mean of the n analysis of the reference material used to calibrate SIMS measurements and $2SD_{LF}^{RM}$ is 2 times the standard deviation (SD) on the reference value of the reference material obtained by laser fluorination. The typical uncertainty on each single unknown analyzes is in the order of 0.2 to 0.3‰ (2SE) and the uncertainty on the reference materials is 0.33‰ (2SD) for UNIL_WM3 and 0.26‰ (2SD) for UNIL_Q1.

This is the peer-reviewed, final accepted version for American Mineralogist, published by the Mineralogical Society of America.
The published version is subject to change. Cite as Authors (Year) Title. American Mineralogist, in press.
DOI: https://doi.org/10.2138/am-2020-7523. http://www.minsocam.org/

White mica reference material (RM) for in situ oxygen isotope analysis

Chemical and oxygen isotope homogeneity tests of RMs

The chemical variability of the white mica samples is assessed through the relative error based on the standard deviation of the mean for major elements (1SD), as well as the standard deviation of the mean on the oxygen isotope composition (2SD). Four white mica species, among them one muscovite (UNIL_WM1) and three phengites (UNIL_WM2, UNIL_WM3 and UNIL_WM4) were selected since they have acceptable chemical (<2% relative for Al, Si, K and <7% relative for Mg and Fe) and isotopic (<0.40‰ 2SD) variations within grain and between grains (Fig. 2). One white mica sample (UNIL_WM3) shows a slightly higher chemical variability (4 % relative for Al and 14 % relative for Mg). UNIL_WM1 consists of several large crystals from a Brazilian pegmatite, UNIL_WM2 are large crystals from a Himalayan micaschist sample, and UNIL_WM3 as well as UNIL_WM4 are crushed separates from Alpine rocks. The white mica RMs cover the compositional range from 3.08 to 3.48 Si p.f.u. and an X_{Mg} from 0.43 to 0.80 (Table 1, Fig. 2A).

The typical repeatability of SIMS oxygen isotope measurements on three to six points in individual white mica grains is between 0.30‰ and 0.40‰ (2SD) (Supplemental Table S1). White mica is notoriously difficult to polish and the reproducibility of SIMS measurement is highly dependent on the quality of the polishing. Laser fluorination $\delta^{18}O$ values are: 10.4 ± 0.06‰ for UNIL_WM1, 5.6 ± 0.04‰ for UNIL_WM2, 7.9 ± 0.09‰ for UNIL_WM3 and 5.3 ± 0.17‰ for UNIL_WM4 (Table 2).

Instrumental Mass Fractionation

Two mounts containing all RMs were used to test for compositional variations of instrumental mass fractionation (IMF). Four calibration sessions were performed with varying analysis

conditions (i.e., primary beam of 1, 1.5 and 2 nA; with a 10µm raster and without raster), in order to reduce the IMF and find the optimal analytical conditions. A ΔIMF of 0.24‰ was achieved with the optimal analytical conditions of 1.5 nA primary beam, without raster (Supplementary material S2). Other analytical conditions gave ΔIMF between 0.58‰ and 0.71‰. Plots of IMF versus major element compositions were tested (Tschermak exchange vector and XMg; Fig. 2, B-D) in order to detect any chemical dependent mass fractionation. However, no relationship between major element composition and IMF was found in the different sessions, even though there is a linear IMF dependency on X_{Mg} for biotite (Siron et al., 2017). In fact, the chemical variations in white mica are small, when compared with biotite, which has a large Mg and Fe variation, for instance. An orientation test was performed in order evaluate IMF due to crystal orientation. One crystal was oriented parallel to the c-axis and two others were oriented perpendicular to the c-axis. No IMF change was detected (Fig. 2C). Difficulties were encountered for the samples mounted parallel to c due to a small thickness of the crystals, which resulted in a small amount of analysis, reducing the reproducibility. Nevertheless, this result is in agreement with tests performed on biotite by Siron et al. (2017), who did not find any orientation-dependent fractionation effect. Despite the lack of obvious compositional dependances for white mica, we recommend using the RM which is chemically closest to that of the compositions of white micas to be measured.

Application to whiteschist and metagranites from the Monte Rosa nappe

Sample description

Three samples were selected for detailed SIMS work: two metagranites and one whiteschist. Sample 16MR23 is an undeformed porphyritic metagranite, called metagranite 1 in this study (Fig. 3A). It contains igneous, large centimeter-sized K-feldspar phenocrysts, plagioclase,

quartz, biotite and muscovite. Metamorphic phengite overgrowths igneous muscovites and is also found as biotite pseudomorphs, in association with titanite ± garnet. Late biotite flakes surround those biotite pseudomorphs. Igneous plagioclase is nearly completely pseudomorphosed by a fine-grained assemblage of zoisite, albite and white mica (Luisier et al., 2019). The cores of the plagioclase pseudomorphs are fine-grained, whereas the rims were recrystallized into a coarser-grained assemblage of Fe-rich clinozoisite, oligoclase and white mica. Accessory phases are zircon, apatite, monazite and ilmenite.

Sample 14MR25 is a little deformed porphyritic metagranite, called metagranite 2 in this study (Fig. 3B). It contains large centimetre-sized igneous K-feldspar phenocrysts. Igneous plagioclase is replaced by an assemblage of clinozoisite, albite and phengite. Igneous quartz is recrystallized into fine-grained seriate interlobate quartz and igneous biotite is totally replaced by a fine-grained assemblage of phengite and titanite. Late, small biotite flakes surround those phengites. Small garnets can be found in association with plagioclase in domains close to former igneous biotite. Chlorite locally replaces the late biotite crystals. Accessory phases are titanite, zircon, apatite, monazite and ilmenite.

Metagranites 1 is located about 80 meters and metagranite 2 about 100 meters away from the whiteschist outcrop and show little to no deformation. The study area is affected by a late deformation event, associated with the exhumation of the Monte Rosa nappe. The deformation is observed as localized shear zones in the metagranite, separating large portions of nearly undeformed metagranite. The relationships between microstructures and mineral assemblage in the deformed metagranites indicate that deformation is related to the greenschist facies overprint, which post-dates peak pressure conditions. This is corroborated by the relative chronology of the deformation and crystallization relationships in the whiteschist, confirming a post (PT)peak deformation event throughout the studied area (see also Vaughan-Hammon et al., 2021).

The whiteschist sample 14MR67 (Fig. 3C) was collected close to the center of the whiteschist pipe. The sample contains big dark blue chloritoid crystals embedded in a matrix of talc, phengite and quartz. This paragenesis is characteristic of the Alpine high-pressure peak metamorphic conditions (Chopin and Monié, 1984; Le Bayon et al., 2006; Luisier et al., 2019). A slight schistosity is defined by phengite and talc, which are deformed, indicating that the peak mineral assemblage is pre-kinematic relatively to this light deformation. The deformation is associated with exhumation (e.g., Pawlig and Baumgartner, 2001). Chlorite and sericitic phengite are found as fine-grained retrograde products, which statically replace chloritoid as rims. Talc is partially replaced by chlorite. The fine-grained sericitic phengite and chlorite are post-kinematic relatively to the main schistosity. Microstructural observations allow to distinguish at least two distinct generations of white mica: the first generation of phengites deformed locally in the main schistosity and belong to the high-pressure paragenesis. The second generation is formed by the fine-grained sericitic phengites, replacing chloritoid on its rim. This retrograde alteration is greenschist facies. Quartz grains are present either as big crystals (Fig. 3C), with sub-grain boundaries reflecting incipient deformation, or as small crystals within the mica-rich domains in the schistosity, or as inclusions in chloritoid. Accessory minerals are zircon, apatite, allanite, rutile, monazite, xenotime and florencite.

Oxygen isotope composition of quartz and phengite

The $\delta^{18}O$ values of igneous muscovite in the metagranite 1 show a range between 9.8‰ and 10.7‰ (Fig. 4A), which is slightly higher than the expected variability with a 2 sigma of 0.4‰. Metamorphic phengites $\delta^{18}O$ values are slightly less enriched in ^{18}O (9.1-10.4‰). The $\delta^{18}O$ range of metamorphic phengite in both metagranite 1 and metagranite 2 is similar. Phengites from whiteschists are characterized by lower $\delta^{18}O$ values (5.2-7.3‰) when compared to the two metagranites, and the range in values is larger. Here, two distinct populations can be

correlated with microtextures. The first population is represented by large phengite flakes with $\delta^{18}O$ values > 6‰ (Fig. 5A). The second population is the smaller sericitic phengite crystals, typically replacing chloritoid. This generation is younger than the large flakes and grow during retrograde chloritoid breakdown. They have $\delta^{18}O$ values < 6‰. The sericitic phengites are typically isolated from quartz crystals.

Quartz $\delta^{18}O$ values in the metagranite 1 range from 13.4 to 14.6‰ (Fig. 4B). This is outside the expected range for a homogeneous distribution with a 2 sigma of 0.3‰. Indeed, the centers of the larger grains, interpreted to be igneous, cluster towards the lower values of that range and the smaller, recrystallized grains, as well as the outer parts of the larger grains, are closer to the upper end of the $\delta^{18}O$ range (Fig. 5B). Fine-grained quartz crystals from the metagranite 2 are homogeneous within uncertainty with values between 13.2 and 13.5‰. Whiteschist quartz has $\delta^{18}O$ values ranging from 9.1 to 10.6‰. No correlation with microtexture was found (Fig. 5A). The $\delta^{18}O$ values of white micas were plotted against their silica content for each white mica generation in Fig. 6A. Large muscovites, interpreted to be igneous in metagranite 1 have silica contents ranging between 3.01 and 3.14 atoms per formula unit (a.p.f.u). They are homogeneous within uncertainty and show the highest $\delta^{18}O$ values. One data point is slightly higher. Metamorphic phengites from metagranite 1 have compositions ranging from 3.03 to 3.17 silica a.p.f.u, which is identical to igneous muscovites. However, they show a wider range in $\delta^{18}O$ values, without a correlation with celadonite composition (Fig. 5B, D). The silica content of phengites in the metagranite 2 are higher than those in metagranite 1 and lie (with one exception) between 3.20 and 3.45 a.p.f.u (Fig. 6A). They have the lowest $\delta^{18}O$ value amongst metagranites, but no clear correlation between Si content and $\delta^{18}O$ was observed. Hence, there is no correlation of $\delta^{18}O$ values with celadonite (e.g., silica) content. Celadonite component is a monitor of pressure at which the phengite formed in granitic mineral assemblages, since the

375 buffer assemblage quartz-k-feldspar-biotite-phengite is present in these granites (e.g.,
376 Massonne and Schreyer, 1987).
377 The oxygen isotopic composition of phengite in whiteschist is plotted as a function of silica
378 content in Fig. 6B. Two groups are visible, low silica content phengites plot around a $\delta^{18}O$ value
379 of 5.2 – 6.0‰, while high silica content phengites plot between 6.1 – 7.2‰. These two groups
380 are reflected in the histograms in Fig. 4A. As outlined above, the low silica phengites are
381 crystals measured in the retrograde sericitic phengite haloes surrounding the chloritoid (see also
382 Fig. 5A, C). Interestingly, there is no dependence of the $\delta^{18}O$ value on silica content of the
383 phengites within each group.
384
385 **White mica - quartz isotope thermometry**
386 Temperatures have been calculated, based on the fractionation between quartz and muscovite
387 and respectively quartz and phengite (Zheng, 1993) for quartz-white mica pairs (Fig. 7) from
388 the same microstructural domains (Table 3).
389 In metagranite 1, quartz-white mica pairs can be separated into two populations: igneous
390 muscovite and quartz pairs and metamorphic phengite and quartz pairs. Igneous pairs result in
391 oxygen isotope fractionation temperatures between 350°C and 450 °C (Table 3, Fig. 7). These
392 values are clearly too low for igneous crystallization temperatures and most likely reflect sub-
393 solidus re-equilibration during cooling of the granite intrusion as is often seen in granitic
394 systems (see e.g., O'Neil et al., 1977) or metamorphic re-equilibration upon cooling after the
395 Alpine metamorphism (see e.g., Eiler et al., 1993). The metamorphic overgrowths and fine-
396 grained phengites in the matrix were paired with the rims of igneous quartz and recrystallized
397 quartz grains and indicate a temperature range of 300 to 330 °C (Fig. 7). Using this temperature
398 range and the phengite content of these mica crystals (3.03 to 3.17; Table 3) results in pressures
399 of less than 0.2 GPa, assuming a H_2O activity of 1 (Massonne and Szpurka, 1997). The

temperature and pressure range for these metamorphic phengites in metagranite 1 suggests a prehnite-actinolite or low temperature greenschist facies.

Metagranite 2 is characterized by metamorphic phengites, replacing igneous biotites. The pseudomorph nature of these domains and the juxtaposition of the pseudomorphs with plagioclase did not allow to find many quartz - phengite pairs that can be assumed to be in isotopic equilibrium based on textural arguments. Nevertheless, a pair with high-silica phengite (3.39) was identified, suggesting it to be a high-pressure mica. It yields a temperature of 350 ± 40 °C (Table 3). The temperature obtained is similar within uncertainty to that of low silica phengites from metagranite 1 (Fig. 7). The maximum silica content of the phengite (3.45) requires pressures of ca. 0.5 GPa at 350 °C (Massonne and Szpurka, 1997). In contrast, if these phengites were formed during peak-temperature, as proposed by Luisier et al. (2019), of 575 °C, this would correspond to a pressure of 1.1 GPa (Massonne and Szpurka, 1997). Then, the temperatures reflected by the oxygen isotope thermometry would also reflect retrograde re-equilibration of the small mica crystals by diffusion upon cooling during the regional Alpine event. The slightly lower temperatures obtained for the small metamorphic crystals would agree with this suggestion (Eiler et al., 1993).

White micas in the whiteschist used for temperature estimation are the high-pressure phengites (Si > 3.38 a.p.f.u). The results span a rather large temperature range with an average of 440 ± 50 °C (Table 3 and Fig. 7). The large variation is due to two effects. On one hand, white mica and quartz oxygen isotope data showed a variability of 0.7‰ and 0.9‰ respectively. On the other hand, uncertainties accumulated by SIMS analysis (0.3‰ for phengite, 0.3‰ for quartz), together with the small temperature dependance of the white mica quartz fractionation for oxygen isotopes, will also lead to large uncertainties of ca. ± 50 °C (assuming an uncertainty of 0.4‰ for the oxygen isotope fractionation measurement). This temperature range partially overlaps with previous temperature estimates of prograde to peak Alpine metamorphic

conditions from the literature (500-575 °C; Chopin and Monié, 1984; Le Bayon et al., 2006; Luisier et al., 2019; Vaughan-Hammon et al., 2021). Slightly lower oxygen isotope fractionation temperatures compared to the peak temperature conditions from the literature could be explained by re-equilibration by diffusion during post-peak, retrograde cooling.

The temperature of the retrograde growth event of the younger white mica generation replacing chloritoid cannot be determined by using quartz - white mica pairs, since quartz is absent from the pseudomorphs. Nevertheless, chlorite-phengite parageneses are typical for greenschist metamorphism (300-450 °C; Bucher and Grapes, 2011).

Discussion

Formation of the whiteschist protolith and its Alpine metamorphic evolution

White mica and quartz oxygen isotope compositions show a significant variation between the whiteschist and metagranites samples, showing that the igneous isotopic compositions were completely reset during metasomatism of the granite to produce the whiteschist protolith. Pawlig and Baumgartner (2001) suggested an argillitic alteration of the Monte Rosa granite by late magmatic fluids, producing the chemistry of the whiteschist protolith by producing a rock composed of sericite, chlorite and quartz. The pre-Alpine age of the metasomatic alteration has been confirmed by Marger et al. (2019), based on the study of chemical and isotopic zoning patterns recorded in tourmaline from whiteschists. Different conclusions were reached by Sharp et al. (1993), based on similar oxygen isotope data on bulk mineral separates from the Dora Maira whiteschist. They suggested a metasomatizing fluid of seawater origin, which was liberated by dehydration of serpentinite. However, the implication of fluids related to the dehydration of mafic to ultramafic rocks in the genesis of the whiteschist protolith has been discussed by Luisier et al. (2021) in detail, based on the geometry of alteration, the major

element and stable isotope composition of bulk rocks, as well as stable isotope information presented in Marger et al. (2019). They confirmed the origin of the fluids to be hydrothermal, pre-high pressure, in the case of the Monte Rosa whiteschist genesis (Luisier et al., 2021).

The difference in isotopic composition for low and high silica phengites shown in Fig. 6A for whiteschist documents a second alteration event, which leads to the formation of the retrograde replacement of chloritoid by white mica. Indeed, the high-pressure mineralogy of the whiteschist was acquired during the Alpine eclogite-facies metamorphism (Chopin and Monié, 1984; Le Bayon et al., 2006; Luisier et al., 2019), inheriting the isotopic and chemical composition of the metasomatized granite. Quartz and chlorite reacted during the prograde increase in P-T, to form talc and chloritoid. This reaction consumes all chlorite over a relatively small P-T-range (see Fig. 8A). In parallel, the celadonite content increased, resulting in a maximum silica content of 3.46 in phengite, in agreement with the isopleths calculated in the stability field of white mica - chloritoid - talc - quartz under H_2O saturated conditions (Fig. 8A). Calculations under H_2O saturated conditions are justified due to the fact that the prograde reactions produce H_2O (Fig. 8B), a fact pointed out by Luisier et al. (2019); and supported by H_2O content measurements by SIMS in the high pressure phengites by Luisier et al. (2019).

Decompression and cooling of the whiteschist will desiccate the grain boundaries. The fact that the peak assemblage is generally well-preserved shows that the retrograde chlorite breakdown reaction to biotite was never crossed. The chlorite to biotite breakdown reaction is a dehydration reaction, producing significant amounts of H_2O as indicated by the rapid drop in H_2O contained in the assemblage (Fig. 8B). Hence decompression was not accompanied by significant heating. Isothermal decompression or cooling during decompression is indicated by the preservation of the whiteschist peak assemblage. The localized, sericitic, low celadonite phengites surrounding chloritoid requires minor infiltration of external fluids. The texture suggests that chloritoid replacement by sericitic phengite happens simultaneously with local chloritization of talc. This

475 retrograde replacement is related to a very localized fluid infiltration. The $\delta^{18}O$ values of the
476 late sericitic phengites are systematically about 1‰ lower than the high-pressure phengites (Fig.
477 6B). The fact that quartz oxygen isotope composition does not show a bimodal composition
478 and that quartz inclusions in the core of chloritoid have the same composition as matrix quartz
479 demonstrates that quartz did not exchange its isotopic composition (Fig. 5A). This is likely due
480 to the fact that the infiltration occurs post-deformation, and quartz is not produced by the
481 retrograde reaction as demonstrated by the absence of quartz in the sericite rims. Resetting by
482 diffusion at these low temperatures suggests that only very small amounts of quartz were
483 precipitated, if at all.
484 The formation of retrograde white micas in the whiteschist is due to chloritoid breakdown, as
485 shown by the microstructural record (Fig. 5A and C). Very fine-grained sericitic phengites
486 replaced chloritoid. These mica crystals have Si content between 3.00 and 3.15 and have $\delta^{18}O$
487 values between 5.2‰ and 6.0‰ (Fig. 6B). The temperature of crystallization for these
488 retrograde sericitic phengites cannot be determined directly from isotopic exchange equilibria,
489 since no quartz in textural equilibrium could be identified. Here, we will assume that this
490 retrograde alteration occurred during the greenschist facies (ca. 450 °C, also suggested by Frey
491 et al., 1976, for the retrograde metamorphic event in the Monte Rosa) or even later, at the same
492 time as the fluids infiltrated metagranite 1, at a temperature of about 315 °C (Table 3). The
493 pressures recorded by these sericitic phengites would be about 0.5 GPa (see Fig. 8A), assuming
494 H_2O saturation. However, since the pseudomorphic replacement is typically arrested, leaving
495 significant amounts of chloritoid and talc in most whiteschist samples, it seems unlikely that
496 H_2O saturation was maintained during retrogression. Indeed, the partial replacement texture
497 indicates that H_2O was fully consumed, suggesting H_2O fugacities significantly below H_2O
498 saturation. Hence, these pressures should be taken with care.

Transforming chloritoid and talc to sericitic phengite and chlorite requires fluid infiltration (see discussion above), since chlorite - phengite paragenesis contain more H_2O than chloritoid and talc assemblages (Fig. 8B). Given the abundance of phengite in the chloritoid alteration halo (Fig. 5A, C), this fluid also introduces potassium. The oxygen isotope composition of the fluids in equilibrium with the sericitic phengites replacing chloritoid have a calculated $\delta^{18}O$ composition ranging between 2.5‰ to 6.0‰ (Zheng, 1993) for a temperature range between 250 to 450 °C, respectively.

At the outcrop scale, the external rim of the whiteschist body is fully retrogressed into a greenschist-facies assemblage. The paragenesis consists of chlorite, muscovite and quartz and in some zones poikilitic albite. Locally, chloritoid pseudomorphs can still be identified. This means that the outer rim of the whiteschist pipe has been much more affected by retrograde fluid influx than the center of the whiteschist. This is not surprising, as lithological contacts represent favorable fluid pathways.

Mechanism of retrograde alteration and origin of late fluids

The isotopic signatures recorded in rocks due to fluid-rock interaction can be used to understand the mechanism of alteration, and, in some cases, the origin of the fluids. Fluid-rock interaction can be classified into two endmember processes: rock-buffered or fluid-buffered (e.g., Baumgartner and Valley, 2001). While fluid-buffered systems allow to determine the composition of the external fluids, this information is lost in systems which are rock dominated. Indeed, rock-buffered systems, in which isotopic equilibrium is maintained for the whole rock are not interesting for isotopic studies, since no changes related to fluid-rock interaction will be observed. Nevertheless, rock-buffered systems can be used very successfully, if partial or local equilibrium or mass balancers are used (e.g., Skora et al., 2011). At any given time in the history of a fluid infiltration system, it can locally be rock-buffered, while other parts of the system are

524 fluid-buffered (e.g., Baumgartner and Rumble, 1988; Bowman et al., 1994), especially if fluid
525 flow is focused in heterogeneous permeability media (e.g., Baumgartner and Valley, 2001; Cui
526 et al., 2001; Gerdes et al., 1995) or by deformation (e.g., Person et al., 2007; Quilichini et al.,
527 2015; Tartèse et al., 2012). Stable isotope compositions in rock-dominated system, while
528 having lost the information on fluid source, can still be used to evaluate the reaction
529 mechanisms in combination with phase petrology and microtexture. Below we present two
530 endmember models based on the above discussion to interpret the retrograde alteration of the
531 whiteschists.
532 *Fluid-buffered model:* The fluids infiltrating the whiteschists have low $\delta^{18}O$ values of 2.5‰ to
533 6.0‰, assuming fluid-buffering and equilibrium of precipitated sericitic phengites at
534 temperatures between 250 and 450 °C, respectively. Fluids with such low $\delta^{18}O$ value cannot
535 originating from the Monte Rosa metagranite or the surrounding paragneisses, since their
536 isotopic composition is much too high as is shown for the granite in this study (see also
537 Darbellay, 2005; Luisier et al., 2021); they have to be external to the Monte Rosa nappe. Other
538 probable sources in the geologic context of the Monte Rosa nappe are Bündnerschiefer from
539 the Zermatt-Saas zone (ZSZ), which can be found at a few hundred meters distance from the
540 whiteschist outcrop discussed here (Fig.1). Nevertheless, the Bündnerschiefer, and the mafic
541 rocks in immediate contact with the nappe, all have higher $\delta^{18}O$ values relatively to the
542 whiteschist (Cartwright and Barnicoat, 1999; Dessimoz, 2005). A more plausible source are the
543 Zermatt-Saas serpentinites, which are abundant in the ZSZ (Steck et al., 2015). Serpentinites
544 from the Zermatt-Saas unit have $\delta^{18}O$ values between 0‰ to 5‰ in the Upper Ayas Valley
545 (Dessimoz, 2005). Fluids equilibrated or produced by these serpentinites would be a suitable
546 source for the low $\delta^{18}O$, in agreement with serpentinites data from other locations in the
547 Zermatt-Saas unit (Cartwright and Barnicoat, 1999). Serpentinites can potentially release a
548 substantial amount of fluids during dehydration reactions, as indicated by the positive slope of

549 the antigorite breakdown reaction in a P-T diagram (Kerrick and Connolly, 2001; Ulmer and
550 Trommsdorff, 1995). Nevertheless, this reaction occurs at significantly higher temperatures
551 than the proposed temperature-pressure path for the Monte Rosa nappe (Luisier et al., 2019;
552 Vaughan-Hammon et al., 2021), so that the fluids would either have traveled a large distance
553 through the nappe stack from hotter parts of the orogen, or that extraneous fluids (surface fluids
554 for example) would have equilibrated with the local serpentinite stack during exhumation (e.g.,
555 Barnes et al., 2004; Philippot and Selverstone, 1991). Hence, while it is not possible to exclude
556 this model, it seems not very likely.
557 *Rock buffered model:* Textural observations show that the new, retrograde sericitic phengite
558 replaces chloritoid (Fig. 3, 5). Sericite dominates the rims and the pseudomorphs, but some
559 chlorite is also found. An isotopic equilibrium between high-pressure phengite at peak
560 metamorphic conditions (570 °C/2.2 GPa; Fig. 8A) with chloritoid can be written as:

561 $$\delta^{18}O_{ctd} = \delta^{18}O_{HPphe} + \Delta^{570°C}_{ctd-HPphe} \quad (3)$$

562 with $\delta^{18}O_{ctd}$ being the $\delta^{18}O$ of chloritoid, $\delta^{18}O_{Hp\text{-}phe}$ the $\delta^{18}O$ of the high-pressure phengite and
563 $\Delta^{570°C}_{ctd-phe}$ the fractionation factor of $\delta^{18}O$ between chloritoid and high-pressure phengite at 570
564 °C. The fractionation factor used, from Zheng (1993), is -0.85‰. Hence, the oxygen isotope
565 composition of chloritoid in equilibrium with the high-pressure phengite would be nearly 1‰
566 lighter than that of the phengite. If we assume that the amount of oxygen supplied by the fluid
567 – e.g., the assumption of rock-buffered system – the newly crystallized phengite inherits its
568 isotopic composition from the chloritoid, it would be roughly 1‰ lighter than the high-pressure
569 sericitic phengites in the whiteschist. This agrees with the data measured: the high-pressure
570 phengites have a composition between 6.1 and 7.5‰, while retrograde, sericitic phengites with
571 low silica content have values of 5.2 to 6.0‰.
572

573 ## Implications

574

575 This study required the development of white mica reference materials covering the phengite
576 solid solution for in situ oxygen isotope measurements by SIMS. Four species, among them
577 one muscovite (UNIL_WM1) and three phengites (UNIL_WM2, UNIL_WM3 and
578 UNIL_WM4) were found to be suitable as reference materials for SIMS analyses. They should
579 allow the measurement of the oxygen isotope composition of most white mica specimen, since
580 no compositional dependance on celadonite content was found. The measurement repeatability
581 is between 0.30 and 0.40‰ when using the optimal analytical conditions of 1.5 nA primary
582 beam, without raster. The RMs are available upon request at the SwissSIMS facility of the
583 University of Lausanne.
584 White micas crystallize over a large range of pressure and temperature conditions and are
585 sensitive markers of fluid-rock interactions. Three Monte Rosa samples, consisting of one
586 whiteschist and two metagranite were selected for in situ SIMS oxygen isotopes measurement
587 of white mica and quartz to investigate fluid-rock interaction leading to metasomatism of
588 granite, the formation of whiteschist and their retrograde alteration. Whiteschist oxygen
589 isotopes compositions in both white mica and quartz are significantly lower than in the
590 metagranite and are not overlapping. Whiteschist chemistry was established before Alpine
591 metamorphism, which resulted in the crystallization of the actual whiteschist paragenesis of
592 talc-chloritoid-phengite-quartz. The temperature estimates for the peak metamorphic
593 conditions with oxygen isotope fractionation between quartz and phengite ranged between 380
594 °C and 540 °C. These are lower than the 570 °C (at 2.2 GPa) obtained using thermodynamic
595 phase petrology modelling. The large T-range observed is mostly due to the analytical
596 uncertainty of ± 0.3‰ for quartz and 0.3‰ for mica. Together with the small temperature
597 dependence of the quartz-phengite fractionation factor, this results in ca. 60 °C (at 300 °C) and
598 120 °C (at 500 °C) uncertainties for individual temperature estimates.

599 Retrograde, sericitic phengites partially replacing chloritoid crystals have lower $\delta^{18}O$ values
600 than the peak phengites. We suggest that only minor amounts of fluid infiltrated the
601 whiteschists, resulting in a local rock buffering of isotopic compositions. The field and textural
602 observations support this rock-buffered model. Sourcing the fluids from the ultramafic rocks of
603 the Zermatt-Saas unit seems unlikely.
604 Larger amounts of externally derived fluids infiltrated along the granite-whiteschist contact,
605 obliterating any chloritoid in these outer zones. In contrast, only minor retrogression is found
606 within the whiteschist body, documenting that inside the body there was only a very limited
607 amount of fluid present. Hence the whiteschist-granite couple acted as a heterogeneous fluid
608 flow system, in which fluid is concentrated at the contact, with only minor retrogression of both
609 granite and whiteschist away from the contact.
610 Our study allowed the distinction of several fluid events at the origin of the oxygen isotope
611 composition of white mica and quartz in the Monte Rosa whiteschist and metagranite. A first
612 major and pervasive event is responsible for the hydrothermal alteration of the granite into the
613 whiteschist, before the onset of Alpine orogeny, and a late, localized, fluid infiltration related
614 to nappe exhumation was characterized. These results highlight the ability of white mica to
615 maintain its chemical and isotopic composition throughout regional metamorphism and
616 localized fluid-rock interactions, further demonstrating that in situ $\delta^{18}O$ measurements in white
617 mica is a powerful tool to monitor changes in environmental growth conditions.
618

619 ## Acknowledgments

620

621 This research was supported by the Swiss National Foundation grants n° 26084159 and
622 206021_163991. We would like to thank Guillaume Siron and Florence Bégué for their help
623 and guidance with SIMS analyses and sample preparation, Torsten Vennemann for giving us

the access to the stable isotope laboratory and Martin Robyr for his assistance with EPMA data acquisition. Katharina Marger and Joshua Vaughan-Hammon and thanked for stimulating discussions. Constructive reviews by Simona Ferrando and one anonymous reviewer are gratefully acknowledged.

References

Bailey, S.W., 1984. Classification and Structures of the Micas, in: Micas, Reviews in Mineralogy. pp. 1–12.

Barnes, J.D., Selverstone, J., Sharp, Z.D., 2004. Interactions between serpentinite devolatilization, metasomatism and strike-slip strain localization during deep-crustal shearing in the Eastern Alps. Journal of Metamorphic Geology 22.

Baumgartner, L.P., Rumble, D., 1988. Transport of stable isotopes: I: Development of a kinetic continuum theory for stable isotope transport. Contr. Mineral. and Petrol. 98, 417–430.

Baumgartner, L.P., Valley, J.W., 2001. Stable Isotope Transport and Contact Metamorphic Fluid Flow. Reviews in Mineralogy and Geochemistry 43, 415–467.

Bearth, P., 1952. Geologie und Petrographie des Monte Rosa. Beitr. Geol. Karte Schweiz NF 96 94 p.

Berman, R.G., 1988. Internally-Consistent Thermodynamic Data for Minerals in the System Na2O-K2O-CaO-MgO-FeO-Fe2O3-Al2O3-SiO2-TiO2-H2O-CO2. J. Petrology 29, 445–522.

Bowman, J.R., Willett, S.D., Cook, S.J., 1994. Oxygen isotopic transport and exchange during fluid flow: One-dimensional models and applications. American Journal of Science; (United States) 294:1.

Bucher, K., Grapes, R., 2011. Metamorphism of Mafic Rocks, in: Bucher, K., Grapes, R. (Eds.), Petrogenesis of Metamorphic Rocks. Springer, Berlin, Heidelberg, pp. 339–393.

649 Bucher-Nurminen, K., Frank, E., Frey, M., 1983. A model for the progressive regional
650 metamorphism of margarite-bearing rocks in the Central Alps. American Journal of
651 Science 283-A, 370–395.
652 Bulle, F., Rubatto, D., Ruggieri, G., Luisier, C., Villa, I.M., Baumgartner, L., 2020. Episodic
653 hydrothermal alteration recorded by microscale oxygen isotope analysis of white mica
654 in the Larderello-Travale Geothermal Field, Italy. Chemical Geology 532, 119288.
655 Cartwright, I., Barnicoat, A.C., 1999. Stable isotope geochemistry of Alpine ophiolites: a
656 window to ocean-floor hydrothermal alteration and constraints on fluid–rock interaction
657 during high-pressure metamorphism. Int Journ Earth Sciences 88, 219–235.
658 Chopin, C., 1985. Les relations de phase dans les métapelites de haute pression. Approche
659 expérimentale et naturaliste, conséquences géodynamiques pour les Alpes occidentales.
660 University Pierre et Marie Curie - Paris VI, Paris.
661 Chopin, C., Monié, P., 1984. A unique magnesiochloritoid-bearing, high-pressure assemblage
662 from the Monte Rosa, Western Alps: petrologic and 40Ar-39Ar radiometric study.
663 Contr. Mineral. and Petrol. 87, 388–398.
664 Coplen, T.B., Kendall, C., Hopple, J., 1983. Comparison of stable isotope reference samples.
665 Nature 302, 236–238.
666 Cui, X., Nabelek, P.I., Liu, M., 2001. Heat and fluid flow in contact metamorphic aureoles with
667 layered and transient permeability, with application to the Notch Peak aureole, Utah.
668 Journal of Geophysical Research: Solid Earth 106, 6477–6491.
669 Dal Piaz, G.V., 2001. Geology of the Monte Rosa massif: historical review and personal
670 comments. Schweizerische Mineralogische und Petrographische Mitteilungen 81, 275–
671 303.
672 Darbellay, B., 2005. Histoire polymétamorphique de la nappe du Mont Rose et contraintes
673 isotopiques., Master Thesis. University of Lausanne, Switzerland.

de Capitani, C., Brown, T.H., 1987. The computation of chemical equilibrium in complex systems containing non-ideal solutions. Geochimica et Cosmochimica Acta 51, 2639–2652.

Dessimoz, M., 2005. Métamorphisme et déformation entre la zone de Zermatt-Saas et la zone du Combin, Val d'Ayas, Italie. Master Thesis. University of Lausanne, Switzerland.

Eiler, J.M., Graham, C., Valley, J.W., 1997. SIMS analysis of oxygen isotopes: matrix effects in complex minerals and glasses. Chemical Geology 138, 221–244.

Eiler, J.M., Valley, J.W., Baumgartner, L.P., 1993. A new look at stable isotope thermometry. Geochimica et Cosmochimica Acta 57, 2571–2583.

Eslinger, E.V., Savin, S.M., Yeh, H.-W., 1979. Oxygen isotope geothermometry of diagenetically altered shales. SEPM Special Publication 26, 113–124.

Ferrando, S., 2012. Mg-metasomatism of metagranitoids from the Alps: genesis and possible tectonic scenarios. Terra Nova 24, 423–436.

Frey, M., Hunziker, J.C., O'Neil, J.R., Schwander, H.W., 1976. Equilibrium-disequilibrium relations in the Monte Rosa Granite, Western Alps: Petrological, Rb-Sr and stable isotope data. Contr. Mineral. and Petrol. 55, 147–179.

Gardien, V., Thompson, A.B., Ulmer, P., 2000. Melting of Biotite + Plagioclase + Quartz Gneisses: the Role of H2O in the Stability of Amphibole. J Petrology 41, 651–666.

Gerdes, M.L., Baumgartner, L.P., Person, M., 1995. Stochastic permeability models of fluid flow during contact metamorphism. Geology 23, 945–948.

Guidotti, C.V., Sassi, F.P., 1998. Petrogenetic significance of Na-K white mica mineralogy: Recent advances for metamorphic rocks. European Journal of Mineralogy 815–854.

Kerrick, D.M., Connolly, J. a. D., 2001. Metamorphic devolatilization of subducted marine sediments and the transport of volatiles into the Earth's mantle. Nature 411, 293–296.

698 Kita, N.T., Huberty, J.M., Kozdon, R., Beard, B.L., Valley, J.W., 2011. High-precision SIMS
699 oxygen, sulfur and iron stable isotope analyses of geological materials: accuracy,
700 surface topography and crystal orientation. Surface and Interface Analysis 43, 427–431.
701 Lacroix, B., Vennemann, T., 2015. Empirical calibration of the oxygen isotope fractionation
702 between quartz and Fe-Mg chlorite. Geochimica Et Cosmochimica Acta 149, 21–31.
703 Lapen, T.J., Johnson, C.M., Baumgartner, L.P., Piaz, G.V.D., Skora, S., Beard, B.L., 2007.
704 Coupling of oceanic and continental crust during Eocene eclogite-facies
705 metamorphism: evidence from the Monte Rosa nappe, western Alps. Contrib Mineral
706 Petrol 153, 139–157.
707 Le Bayon, R., Capitani, C. de, Frey, M., 2006. Modelling phase–assemblage diagrams for
708 magnesian metapelites in the system K2O–FeO–MgO–Al2O3–SiO2–H2O:
709 geodynamic consequences for the Monte Rosa nappe, Western Alps. Contrib Mineral
710 Petrol 151, 395–412.
711 Luisier, C., Baumgartner, L., Schmalholz, S.M., Siron, G., Vennemann, T., 2019. Metamorphic
712 pressure variation in a coherent Alpine nappe challenges lithostatic pressure paradigm.
713 Nature Communications 10, 1–11.
714 Luisier, C., Baumgartner, L.P., Putlitz, B., Vennemann, T., 2021. Whiteschist genesis through
715 metasomatism and metamorphism in the Monte Rosa nappe (Western Alps). Contrib
716 Mineral Petrol 176, 10.
717 Marger, K., Luisier, C., Baumgartner, L.P., Putlitz, B., Dutrow, B.L., Bouvier, A.-S., Dini, A.,
718 2019. Origin of Monte Rosa whiteschist from in-situ tourmaline and quartz oxygen
719 isotope analysis by SIMS using new tourmaline reference materials. American
720 Mineralogist 104, 1503–1520.
721 Massonne, H.-J., Schreyer, W., 1987. Phengite geobarometry based on the limiting assemblage
722 with K-feldspar, phlogopite, and quartz. Contr. Mineral. and Petrol. 96, 212–224.

723 Massonne, H.-J., Szpurka, Z., 1997. Thermodynamic properties of white micas on the basis of
724 high-pressure experiments in the systems K2O-MgO-Al2O3-SiO2-H2O and K2O-FeO-
725 Al2O3-SiO2-H2O. Lithos 41, 229–250.
726 O'Neil, J.R., Shaw, S.E., Flood, R.H., 1977. Oxygen and hydrogen isotope compositions as
727 indicators of granite genesis in the New England Batholith, Australia. Contr. Mineral.
728 and Petrol. 62, 313–328.
729 Pattison, D. R. M., Harte, B., 1991. Petrography and Mineral Chemistry of Pelites, in: Voll, G.,
730 Töpel, J., Pattison, David R. M., Seifert, F. (Eds.), Equilibrium and Kinetics in Contact
731 Metamorphism: The Ballachulish Igneous Complex and Its Aureole. Springer, Berlin,
732 Heidelberg, pp. 135–179.
733 Pawlig, S., 2001. Geological Evolution of the Monte Rosa: Constraints from Geochronology
734 and Geochemistry of a Talc-Kyanite-Chloritoid Shear Zone within the Monte Rosa
735 Granite (Monte Rosa Nappe, Italian Western Alps). Thesis. University of Mainz,
736 Germany.
737 Pawlig, S., Baumgartner, L.P., 2001. Geochemistry of a talc-kyanite-chloritoid shear zone
738 within the Monte Rosa granite, Val d'Ayas, Italy. Schweizerische mineralogische und
739 petrographische Mitteilungen 81, 329–346.
740 Person, M., Mulch, A., Teyssier, C., Gao, Y., 2007. Isotope transport and exchange within
741 metamorphic core complexes. American Journal of Science 307, 555–589.
742 Philippot, P., Selverstone, J., 1991. Trace-element-rich brines in eclogitic veins: implications
743 for fluid composition and transport during subduction. Contr. Mineral. and Petrol. 106,
744 417–430.
745 Quilichini, A., Siebenaller, L., Nachlas, W.O., Teyssier, C., Vennemann, T.W., Heizler, M.T.,
746 Mulch, A., 2015. Infiltration of meteoric fluids in an extensional detachment shear zone

(Kettle dome, WA, USA): How quartz dynamic recrystallization relates to fluid-rock interaction. Journal of Structural Geology 71, 71–85.

Rieder, M., Cavazzini, G., D'yakonov, Y.S., Frank-Kamenetskii, V.A., Gottardi, G., Guggenheim, S., Koval, P.V., Mueller, G., Neiva, A.M.R., Radoslovich, E.W., Robert, J.L., Sassi, F.P., Takeda, H., Weiss, Z., Wones, D.R., 1999. Nomenclature of the micas. Mineralogical Magazine 63, 267–279.

Schreyer, P.D.W., 1974. Whiteschist, a new type of metamorphic rock formed at high pressures. Geol Rundsch 63, 597–609.

Schreyer, W., 1973. Whiteschist: A High-Pressure Rock and its Geologic Significance. The Journal of Geology 81, 735–739.

Seitz, S., Baumgartner, L.P., Bouvier, A.-S., Putlitz, B., Vennemann, T., 2017. Quartz Reference Materials for Oxygen Isotope Analysis by SIMS. Geostand Geoanal Res 41, 69–75.

Sharp, Z.D., Essene, E.J., Hunziker, J.C., 1993. Stable isotope geochemistry and phase equilibria of coesite-bearing whiteschists, Dora Maira Massif, western Alps. Contr. Mineral. and Petrol. 114, 1–12.

Siron, G., Baumgartner, L., Bouvier, A.-S., Putlitz, B., Vennemann, T., 2017. Biotite Reference Materials for Secondary Ion Mass Spectrometry 18O/16O Measurements. Geostandards and Geoanalytical Research 41.

Skora, S., Baumgartner, L.P., Vennemann, T.W., 2011. Modelling changes in stable isotope compositions of minerals during net transfer reactions in a contact aureole: Wollastonite growth at the northern Hunter Mountain Batholith (Death Valley National Park, USA). Chemical Geology 289, 197–209.

770 Skora, S., Blundy, J., 2010. High-pressure Hydrous Phase Relations of Radiolarian Clay and
771 Implications for the Involvement of Subducted Sediment in Arc Magmatism. J
772 Petrology 51, 2211–2243.
773 Skora, S., Mahlen, N.J., Johnson, C.M., Baumgartner, L.P., Lapen, T.J., Beard, B.L., Szilvagyi,
774 E.T., 2015. Evidence for protracted prograde metamorphism followed by rapid
775 exhumation of the Zermatt-Saas Fee ophiolite. J. Metamorph. Geol. 33, 711–734.
776 Spear, F.S., 1995. Metamorphic Phase Equilibria and Pressure-Temperature-Time Paths.,
777 Mineralogical Society of America. ed. Mineralogical Society of America.
778 Steck, A., Masson, H., Robyr, M., 2015. Tectonics of the Monte Rosa and surrounding nappes
779 (Switzerland and Italy): Tertiary phases of subduction, thrusting and folding in the
780 Pennine Alps. Swiss J Geosci 108, 3–34.
781 Tartèse, R., Boulvais, P., Poujol, M., Chevalier, T., Paquette, J.-L., Ireland, T.R., Deloule, E.,
782 2012. Mylonites of the South Armorican Shear Zone: Insights for crustal-scale fluid
783 flow and water–rock interaction processes. Journal of Geodynamics, Geodynamics and
784 Orogenesis 56–57, 86–107.
785 Ulmer, P., Trommsdorff, V., 1995. Serpentine Stability to Mantle Depths and Subduction-
786 Related Magmatism. Science 268, 858–861.
787 Valley, J.W., Kita, N.T., 2009. In situ oxygen isotope geochemistry by ion microprobe. MAC
788 short course: secondary ion mass spectrometry in the earth sciences 41, 19–63.
789 Vaughan-Hammon, J.D., Luisier, C., Baumgartner, L.P., Schmalholz, S.M., n.d. Peak Alpine
790 metamorphic conditions from staurolite-bearing metapelites in the Monte Rosa nappe
791 (Central European Alps) and geodynamic implications. Journal of Metamorphic
792 Geology 2021. https://doi.org/10.1111/jmg.12595
793 Zheng, Y.-F., 1993. Calculation of oxygen isotope fractionation in hydroxyl-bearing silicates.
794 Earth and Planetary Science Letters 120, 247–263.

This is the peer-reviewed, final accepted version for American Mineralogist, published by the Mineralogical Society of America.
The published version is subject to change. Cite as Authors (Year) Title. American Mineralogist, in press.
DOI: https://doi.org/10.2138/am-2020-7523. http://www.minsocam.org/

795

796

Figures and tables

Table 1 Major and minor element composition (wt%) of white mica reference materials with structural formula. calculated on a basis of 22 charges

UNIL RM	**UNIL_WM1**		**UNIL_WM2**		**UNIL_WM3**		**UNIL_WM4**	
	average (n=25)	1SD[a]	average (n=25)	1SD[a]	average (n=25)	1SD[a]	average (n=25)	1SD[a]
SiO_2	46.35	0.18	51.49	0.17	49.31	0.53	51.02	0.26
TiO_2	0.44	0.09	0.52	0.03	0.30	0.07	0.20	0.01
Al_2O_3	35.26	0.09	24.42	0.20	28.28	1.14	27.04	0.42
FeO	1.13	0.06	2.91	0.11	3.67	0.29	1.66	0.08
MgO	0.84	0.06	4.04	0.08	1.52	0.21	3.76	0.24
CaO	0.00	0.01	0.00	0.00	0.00	0.00	0.00	0.00
Na_2O	0.81	0.03	0.18	0.04	0.11	0.04	0.53	0.06
K_2O	10.58	0.05	11.33	0.05	11.58	0.10	11.05	0.12
F	0.15	0.04	0.00	0.00	0.00	0.00	0.00	0.00
Cl	0.00	0.00	0.00	0.00	0.00	0.00	0.00	0.00
Total	**95.56**		**94.90**		**94.78**		**95.26**	
Si (T)	3.082	0.012	3.479	0.011	3.350	0.036	3.407	0.018
Al (T)	0.918	0.012	0.521	0.011	0.650	0.036	0.593	0.018
sum T	**4.000**		**4.000**		**4.000**		**4.000**	
Ti (O)	0.022	0.005	0.027	0.002	0.016	0.003	0.010	0.001
Al (O)	1.845	0.015	1.424	0.010	1.615	0.058	1.536	0.025
Fe (O)	0.063	0.003	0.165	0.006	0.208	0.016	0.093	0.005
Mg (O)	0.084	0.006	0.407	0.008	0.154	0.021	0.374	0.024
Mn (O)	0.000	0.000	0.000	0.000	0.000	0.000	0.000	0.000
Cr (O)	0.000	0.000	0.000	0.000	0.000	0.000	0.000	0.000
Ni (O)	0.000	0.000	0.000	0.000	0.000	0.000	0.000	0.000
sum O	**2.013**		**2.022**		**1.993**		**2.013**	
Ca (A)	0.000	0.000	0.000	0.000	0.000	0.000	0.000	0.000
Na (A)	0.104	0.004	0.024	0.005	0.015	0.005	0.068	0.008
K (A)	0.897	0.005	0.976	0.005	1.003	0.009	0.941	0.010
sum A	**1.002**		**1.000**		**1.018**		**1.010**	

[a] Uncertainty expressed as 1SD

797

798

799

800

801

This is the peer-reviewed, final accepted version for American Mineralogist, published by the Mineralogical Society of America.
The published version is subject to change. Cite as Authors (Year) Title. American Mineralogist, in press.
DOI: https://doi.org/10.2138/am-2020-7523. http://www.minsocam.org/

802

Table 2 Oxygen isotope composition of white mica reference materials by laser fluorination

UNIL RM		**UNIL_WM1**	
Date	corrected $\delta^{18}O$ ‰	1SD[a]	n
15-April-2016	10.43	± 0.10	1
16-April-2016	10.36	± 0.01	2
28-October-2016	10.36	± 0.10	2
Average	**10.37**	**± 0.06**	**5**

UNIL RM		**UNIL_WM2**	
Date	corrected $\delta^{18}O$ ‰	1SD[a]	n
16-April-2016	5.67	± 0.10	1
21-March-2018	5.63	± 0.04	3
Average	**5.64**	**± 0.04**	**4**

UNIL RM		**UNIL_WM3**	
Date	corrected $\delta^{18}O$ ‰	1SD[a]	n
15-April-2016	7.85	± 0.05	2
21-March-2018	7.98	± 0.08	2
Average	**7.91**	**± 0.09**	**4**

UNIL RM		**UNIL_WM4**	
Date	corrected $\delta^{18}O$ ‰	1SD[a]	n
15-April-2016	5.40	± 0.25	2
28-October-2016	5.23	± 0.02	2
Average	**5.32**	**± 0.17**	**4**

Standard	**NBS-28**		
Date	$\delta^{18}O$ ‰	1SD[a]	n
15-April-2016	9.86	± 0.05	3
16-April-2016	9.51	± 0.11	4
28-October-2016	9.56	± 0.03	3
21-March-2018	9.49	± 0.02	5

[a] Uncertainty is expressed as 1SD

803

804

805

806

807

This is the peer-reviewed, final accepted version for American Mineralogist, published by the Mineralogical Society of America.
The published version is subject to change. Cite as Authors (Year) Title. American Mineralogist, in press.
DOI: https://doi.org/10.2138/am-2020-7523. http://www.minsocam.org/

Table 3 White mica and quartz SIMS data used as pairs for temperature calculation, based on the quartz-muscovite and quartz-phengite fractionation coefficients from Zheng (1993)

White mica	Species	Si (p.f.u)	$\delta^{18}O$ ‰	2SD[a]	Quartz	$\delta^{18}O$ ‰	2SD[a]	T (°C)	± (°C)
Metagranite 1									
16MR23@31	muscovite	3.02	10.2	0.29	16MR23_qz@05	14.2	0.32	403	48
16MR23@35	muscovite	3.01	10.4	0.28	16MR23_qz_2@05	14.1	0.26	443	50
16MR23@47	muscovite	3.05	9.2	0.27	16MR23_qz@13	13.7	0.25	343	34
16MR23@48	muscovite	3.03	10.5	0.25	16MR23_qz@14	13.9	0.34	463	59
16MR23@30	muscovite	3.12	10.8	0.30	16MR23_qz_2@1	14.4	0.22	435	48
16MR23@40	muscovite	3.17	10.3	0.20	16MR23_qz_2@04	13.9	0.33	443	50
16MR23@32	muscovite	3.04	10.1	0.27	16MR23_qz@05	14.2	0.32	387	46
Average temperature of igneous muscovites								**404**	**42**
16MR23@36	phengite	3.06	9.9	0.25	16MR23_qz_2@06	14.3	0.25	317	33
16MR23@38	phengite	3.04	10.1	0.25	16MR23_qz_2@06	14.3	0.25	326	34
16MR23@16	phengite	3.13	10.2	0.31	16MR23_qz_2@09	14.6	0.26	310	36
16MR23@25	phengite	3.13	9.8	0.20	16MR23_qz@10	14.3	0.25	305	28
16MR23@26	phengite	3.12	9.6	0.29	16MR23_qz@11	13.9	0.32	320	40
16MR23@29	phengite	3.13	9.9	0.28	16MR23_qz_2@02	14.3	0.29	309	35
Average temperature of metamorphic phengites								**314**	**8**
Metagranite 2									
14MR25@19	phengite	3.39	9.5	0.27	14MR25_qz@2	13.5	0.32	349	43
Whiteschist									
14MR67@19	phengite	3.26	6.7	0.25	14MR67_qz@16	9.8	0.26	477	57
14MR67@36	phengite	3.32	7.3	0.22	14MR67_qz@06	10.2	0.28	498	61
14MR67@40	phengite	3.34	6.3	0.16	14MR67_qz@18	9.9	0.22	391	34
14MR67@21	phengite	3.38	7.1	0.21	14MR67_qz@16	9.8	0.26	537	64
14MR67@29	phengite	3.40	6.9	0.25	14MR67_qz@12	10.3	0.26	428	49
14MR67@30	phengite	3.41	6.9	0.19	14MR67_qz@12	10.3	0.26	430	45
14MR67@33	phengite	3.42	6.4	0.31	14MR67_qz@10	10.1	0.28	380	48
14MR67@31	phengite	3.42	6.9	0.23	14MR67_qz_2@10	10.2	0.20	446	43
14MR67@34	phengite	3.42	6.9	0.25	14MR67_qz@10	10.1	0.28	453	56
14MR67@25	phengite	3.42	6.9	0.22	14MR67_qz@13	10.1	0.29	462	55
14MR67@26	phengite	3.42	7.1	0.23	14MR67_qz@13	10.1	0.29	490	61
14MR67@22	phengite	3.42	6.8	0.29	14MR67_qz@14	9.7	0.24	495	64
14MR67@32	phengite	3.43	7.1	0.26	14MR67_qz@11	9.9	0.22	514	60
14MR67@37	phengite	3.43	7.0	0.25	14MR67_qz@05	10.6	0.24	403	44
14MR67@24	phengite	3.46	6.8	0.30	14MR67_qz@13	10.1	0.29	443	60
Average temperature of phengites with 3.38 ≦ Si (p.f.u) ≦ 3.46								**443**	**46**

[a]Uncertainty expressed as 2SD

808

809

This is the peer-reviewed, final accepted version for American Mineralogist, published by the Mineralogical Society of America.
The published version is subject to change. Cite as Authors (Year) Title. American Mineralogist, in press.
DOI: https://doi.org/10.2138/am-2020-7523. http://www.minsocam.org/

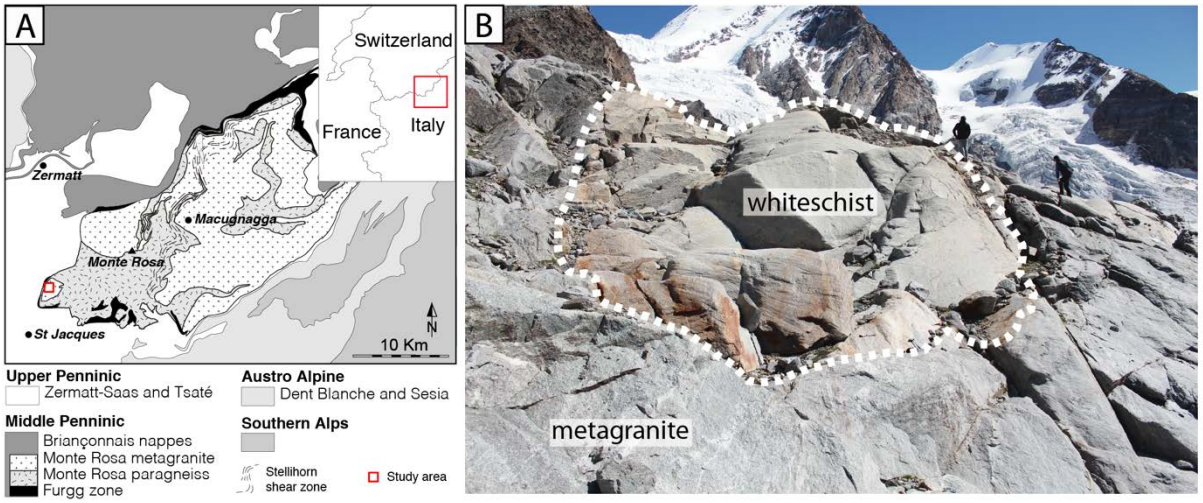

810

811 **Figure 1. A)** Tectonic map showing the geology of the Monte Rosa nappe within the Western
812 Alpine framework (Modified after Steck et al., 2015). **B)** Picture of the whiteschist outcrop.
813 The transition zone with the surrounding metagranite is marked by the white dashed line.

814

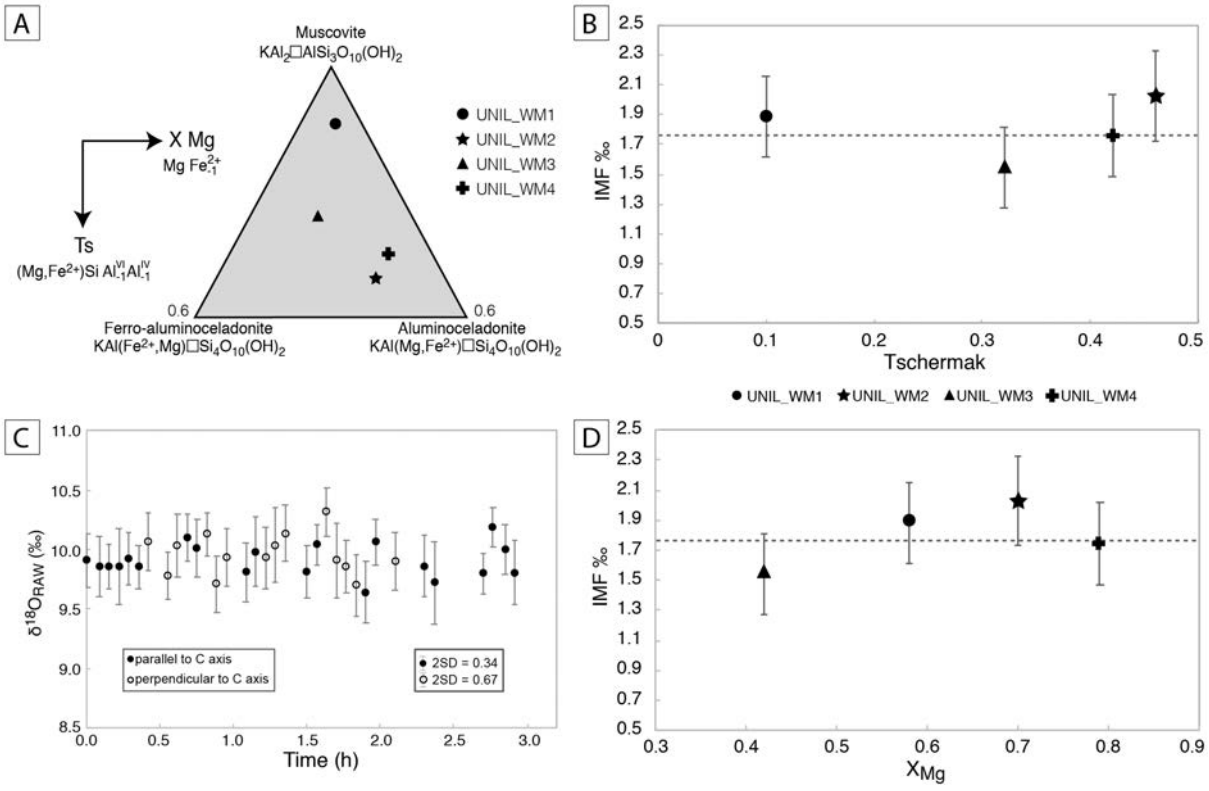

815

816 **Figure 2. A)** Potassium white mica classification triangle of Rieder et al. (1999), showing the
817 muscovite end-member and the theoretical aluminoceladonite and ferro-aluminoceladonite end
818 members. The triangle displays the potential compositional range of natural phengites (Guidotti

819 and Sassi, 1998). Solid symbols are the compositions of the white mica reference materials
820 (RMs) developed in this study. **B** A plot of instrumental mass fractionation (IMF) as a function
821 of Tschermak exchange vector ($Si^{IV}(Mg,Fe)^{VI} = Al^{IV}Al^{VI}$)for the RMs. The IMF is calculated
822 as: IMF = $\delta^{18}O$(SIMS) - $\delta^{18}O$ (Laser Fluorination). **C)** Orientation test performed on three
823 grains of UNIL_WM1. One grain was oriented such that the analyses were performed parallel
824 to the C axis, the two others were oriented for analysis perpendicular to the C axis. Error bars
825 indicate 2SE, i.e., two times the standard error on the mean of the 20 cycles measured for each
826 data point. Note that no IMF was detected, however the large scatter in $\delta^{18}O$ in the crystals
827 oriented perpendicular to the C axis is due to their thin width and the presence of some epoxy
828 between the mica sheets, therefore some analyses were done slightly on epoxy. **D)** Finally,
829 IMF was plotted versus X(Mg). At the level of the precision of measurement of ca. 0.4‰ 2SE
830 it is not possible to see a compositional dependance of the IMF, since the largest and the
831 smallest values determined differ by 0.58‰ (see text for details).
832

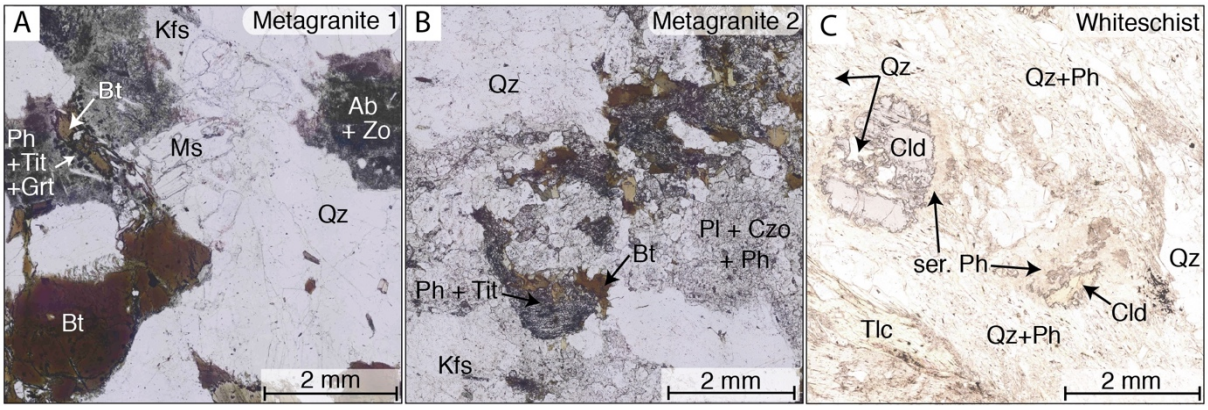

833

834 **Figure 3** Thin sections photomicrographs in plane-polarized light illustrating the main
835 petrographic characteristics of the samples investigated. A) Metagranite 1 is an undeformed
836 porphyritic K-feldspar metagranite, with igneous biotite, muscovite, quartz and K-feldspar.
837 Igneous plagioclase is pseudomorphosed by a fine-grained assemblage of albite + zoisite.
838 Phengite + titanite + garnet form a reaction rim around biotite, when in contact with plagioclase

pseudomorphs. B) Metagranite 2 shows a more pronounced transformation, leaving only quartz and K-feldspar as igneous phases. Plagioclase was replaced by albite + clinozoisite + phengite. Biotite is completely replaced by a fine-grained assemblage of phengite and titanite, locally rimmed by retrograde biotite. C) The whiteschist is composed of chloritoid, talc, phengite and quartz. A slight foliation is marked by the phengite. Chloritoid is partially replaced by a fine-grained assemblage of sericitic phengite and chlorite. Mineral abbreviations are: Ab: albite, Bt: biotite, Cld: chloritoid, Czo: clinozoisite, Grt: garnet, Kfs: K-feldspar, Ms: muscovite, Ph: phengite, Pl: plagioclase, ser. Ph: sericitic phengite, Tlc: talc, Tit: titanite, Zo: zoisite.

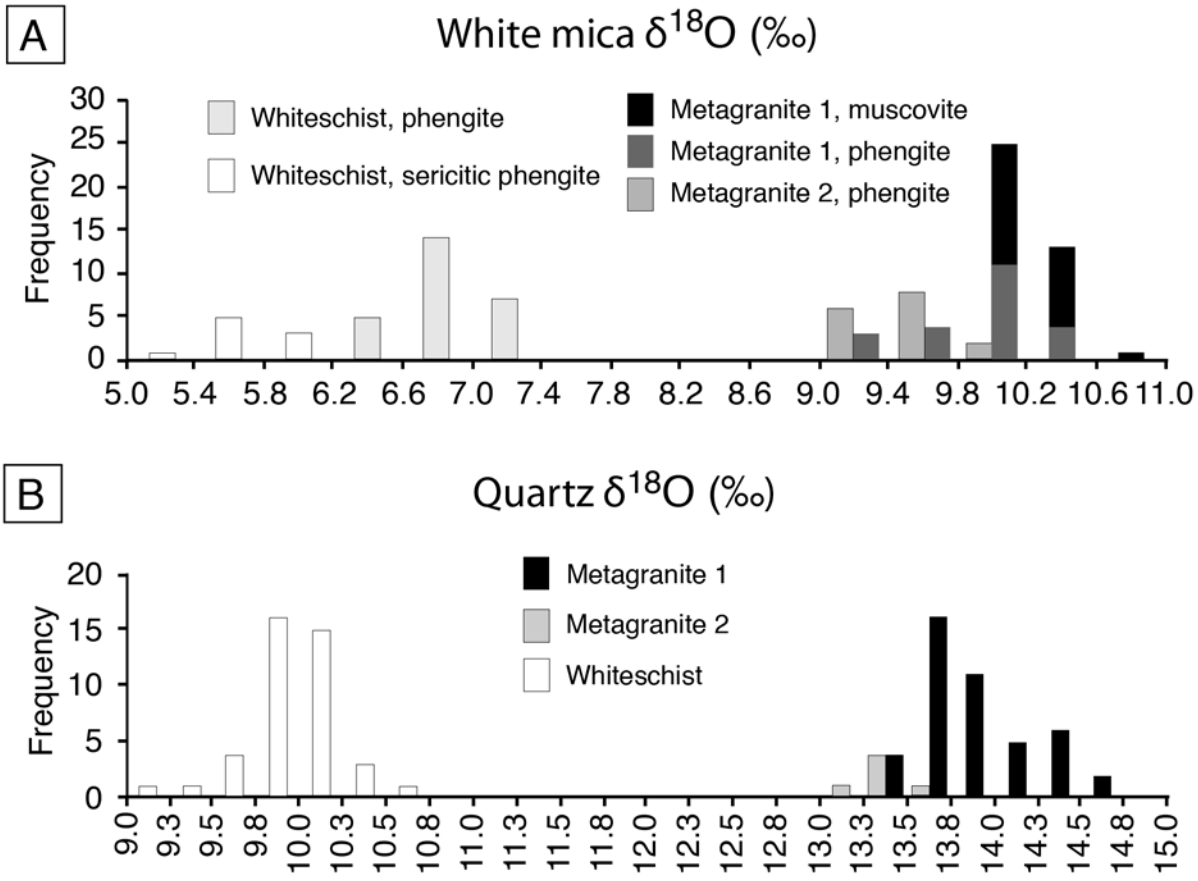

Figure 4. Histograms of $\delta^{18}O$ values measured in white mica (**A**) and quartz (**B**) in different microstructural domains of the metagranite 1, metagranite 2 and the whiteschist. Analyses of igneous muscovite (metagranite 1) and phengites (metagranites 1 and 2) show different values. Note the pronounced difference of isotopic composition of high pressure phengites and retrograde sericitic phengite in whiteschist. The range of each class corresponds to the standard

853 deviation (2SD) of the reference materials analyses, corresponding to 0.34‰ in phengite and
854 0.26‰ in quartz (both 2SE values). Whiteschist has – both in white mica and quartz - a
855 significantly lower oxygen isotopes composition than the metagranites, which are the protoliths
856 for the whiteschist (Luisier et al., 2021). Metagranite 1 and 2 show overlapping $\delta^{18}O$
857 compositions, however in metagranite 2 the $\delta\ ^{18}O$ values are at the lower range of the
858 metagranite spectrum.
859

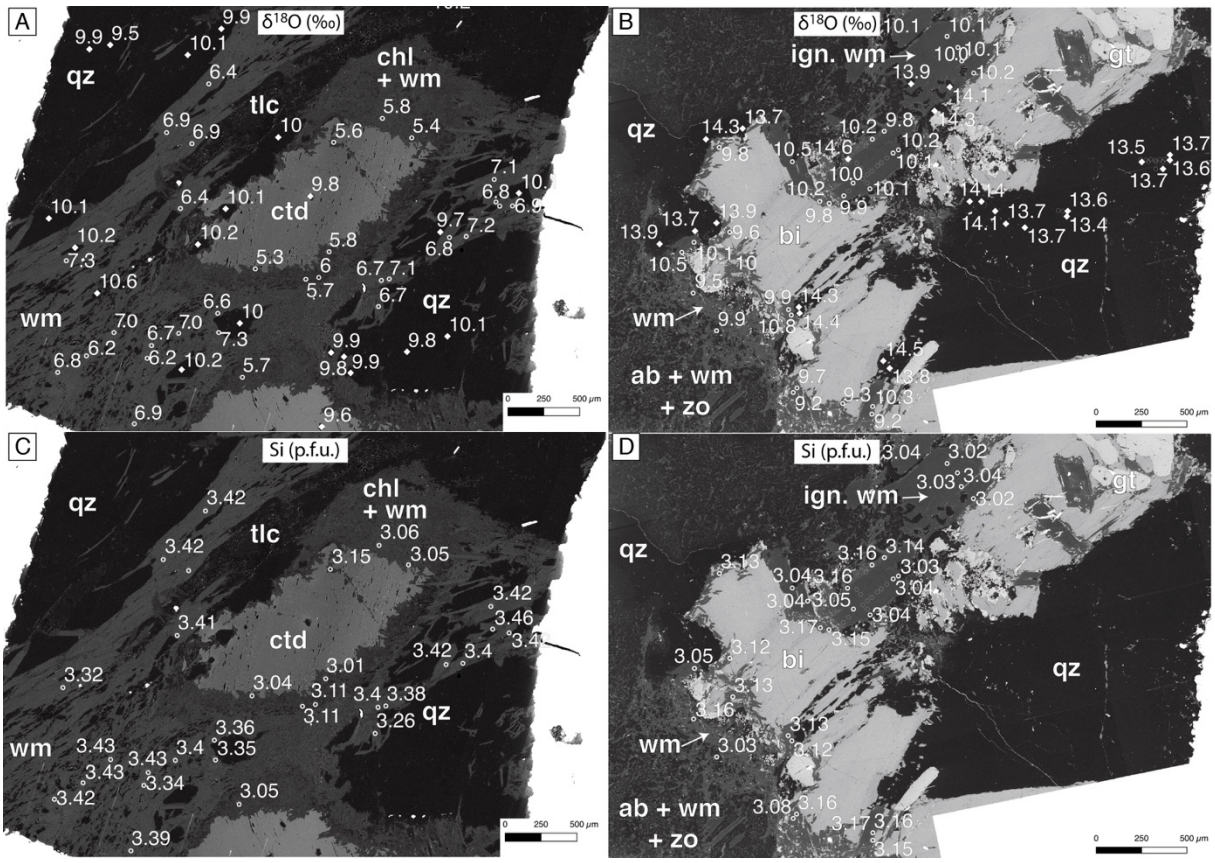

860

861 **Figure 5.** SIMS $\delta^{18}O$ data in ‰ for white mica (dots) and quartz (diamonds) are plotted onto
862 BSE diagrams. Also given is the silica content per formula unit (p.f.u.) of white mica. **A)** $\delta^{18}O$
863 of white mica and quartz from the whiteschist (sample 14MR67) **B)** $\delta^{18}O$ (‰) of white mica
864 and quartz from the metagranite 1 (sample 16MR23) **C)** Si (p.f.u.) content of white mica in
865 whiteschist (14MR67) **D)** Si (p.f.u.) content of white mica in metagranite 1. Large igneous
866 white micas have metamorphic overgrowths of fine grains. Mineral abbreviations are: ab:

This is the peer-reviewed, final accepted version for American Mineralogist, published by the Mineralogical Society of America.
The published version is subject to change. Cite as Authors (Year) Title. American Mineralogist, in press.
DOI: https://doi.org/10.2138/am-2020-7523. http://www.minsocam.org/

867 albite; bi: biotite; chl: chlorite; ctd: chloritoid; gt: garnet; ign. wm: igneous white mica; qz:
868 quartz; tlc: talc; wm: white mica; zo: zoisite.
869

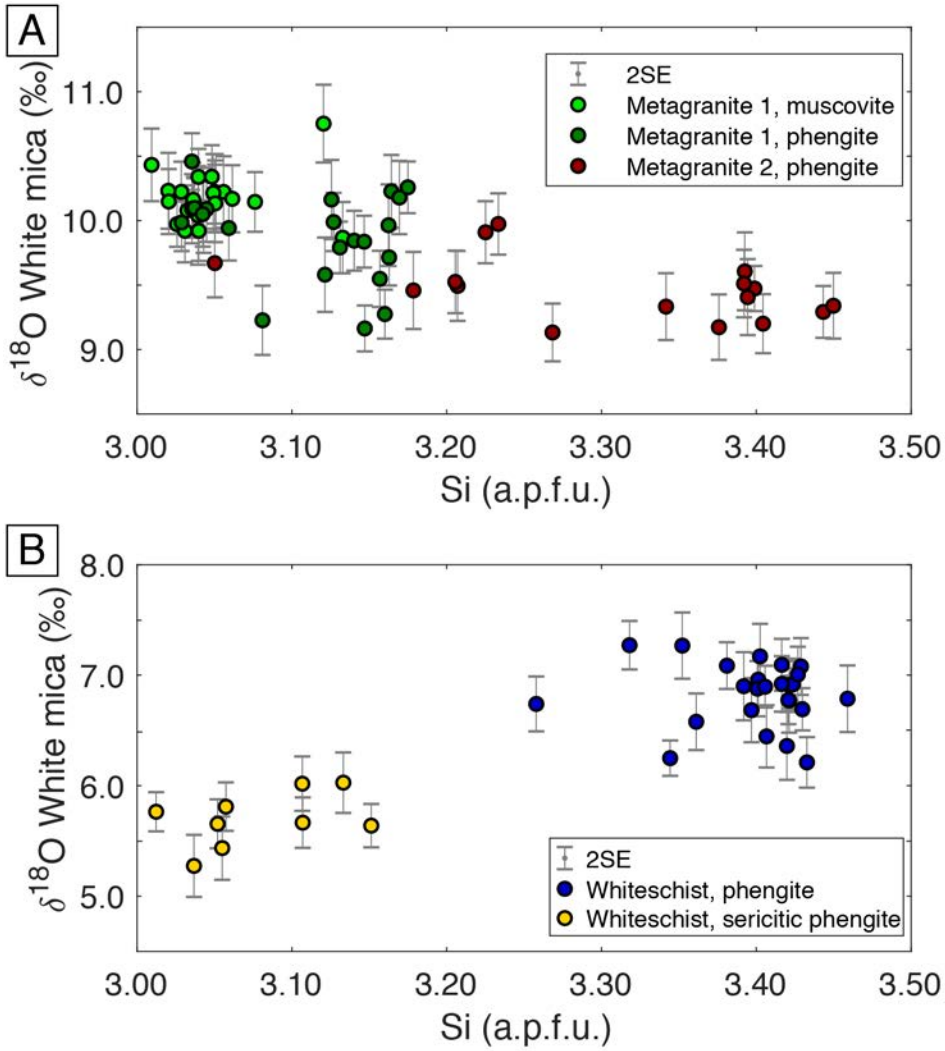

870

871 **Figure 6.** White mica oxygen isotope composition were plotted against the silica content of
872 white mica (a.p.f.u.): for **A**) metagranite 1 and 2 and **B**) whiteschist. Error bars indicate the
873 uncertainty and is expressed as 2SE (‰). Note the isotopic composition of phengite do not
874 correlate with phengite contents in the metagranites, in contrast to a well distinguished change
875 in composition in the whiteschists. Two different groups are defined in the whiteschist, in
876 chemical composition and isotope composition.
877

This is the peer-reviewed, final accepted version for American Mineralogist, published by the Mineralogical Society of America.
The published version is subject to change. Cite as Authors (Year) Title. American Mineralogist, in press.
DOI: https://doi.org/10.2138/am-2020-7523. http://www.minsocam.org/

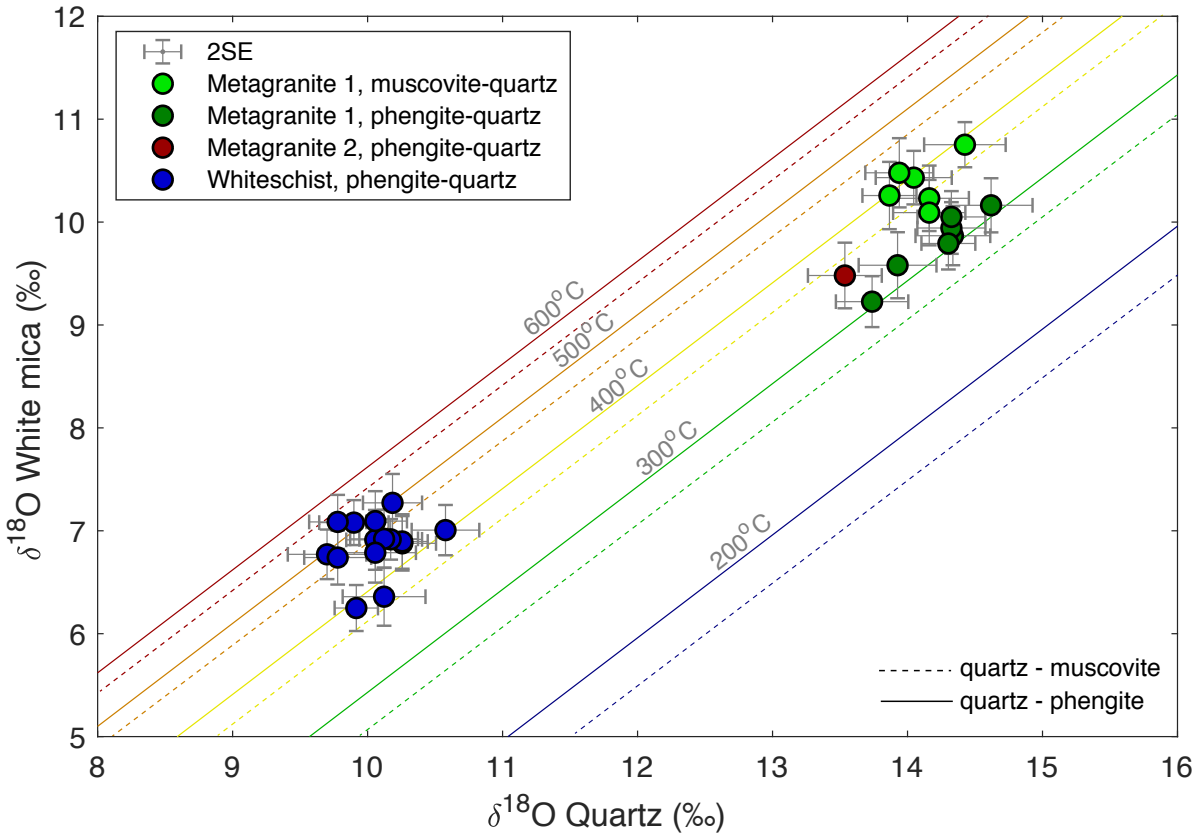

Figure 7. $\delta^{18}O$ of quartz versus $\delta^{18}O$ of white mica plotted for pairs of white mica and quartz, measured in selected microstructural domains were the mineral pairs from the same textural domains. Error bars show the uncertainty (2SE). Temperature isolines were calculated based on the fractionation coefficients between quartz and phengite (solid lines; Zheng, 1993) as well as quartz and muscovite (dashed lines; Zheng, 1993). The whiteschist pairs define a tight cluster around 450°C. The size of the cluster is mainly defined by analytical uncertainties. Only data for high-pressure phengites could be used, since no quartz is found in the retrograde alteration rims of chloritoid. Note that metagranite 2 phengite-quartz pairs display a weak trend parallel to the isolines, suggesting that isotopic equilibrium seems to have been attained between $\delta^{18}O$ of quartz and white mica at a temperature of ca. 350°C.

This is the peer-reviewed, final accepted version for American Mineralogist, published by the Mineralogical Society of America.
The published version is subject to change. Cite as Authors (Year) Title. American Mineralogist, in press.
DOI: https://doi.org/10.2138/am-2020-7523. http://www.minsocam.org/

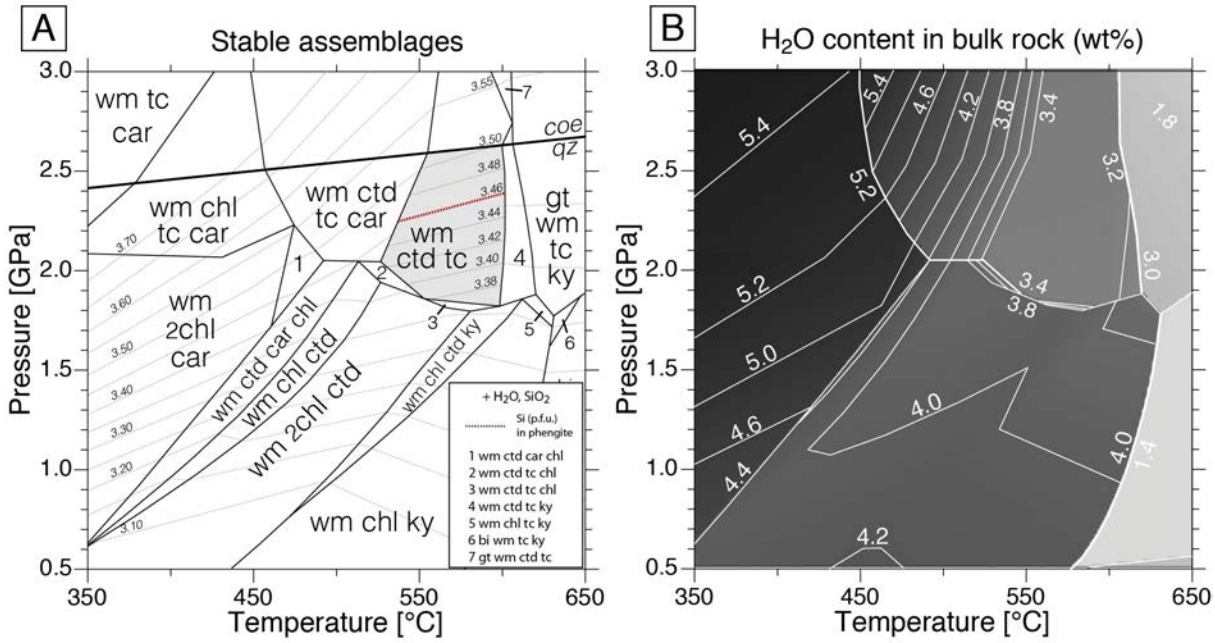

Figure 8. Thermodynamic modelling of the stable assemblages for whiteschist sample 14MR67 in the system KFMASH. The composition used is (in mole): Si(66.02), Al(18.65), Fe(1.73), Mg(9.69), K(3.91). Water saturated conditions were assumed. Quartz is present in all fields. **A**) pressure (P) and temperature (T) diagram representing the stable assemblages. The peak pressure and temperature field is highlighted in grey and the dotted lines represent the silica content of the white mica, with the 4.6 Si p.f.u. isoplet highlighted in bold in the peak P-T field. The peak P-T conditions reached during Alpine metamorphism are min. 2.2 GPa and ca. 570 °C, with the corresponding mineral mode at 2.2 GPa and 570 °C: phengite: 27%, chloritoid: 18%, talc: 10% and quartz: 45%. **B**) P-T diagram displaying the total H_2O content of solid phases, in wt%. The peak P-T field coincides with a major dehydration reaction along the prograde evolution of the rock.